Article No. jmbi.1998.2304 available online at http://www.idealibrary.com on IDEAL J. Mol. Biol. (1999) 285, 595–608

JMB

Three-dimensional Analysis of the 16 nm Urothelial Plaque Particle: Luminal Surface Exposure, Preferential Head-to-head Interaction, and Hinge Formation

Bechara Kachar[1], Fengxia Liang[2], Ulysses Lins[1,3], Mingxiao Ding[2,4] Xue-Ru Wu[5,6], Daniel Stoffler[7], Ueli Aebi[7] and Tung-Tien Sun[2,8]*

[1]*Section on Structural Cell Biology, National Institute on Deafness and other Communication Disorders National Institutes of Health Bethesda, MD 20892, USA*

[2]*Epithelial Biology Unit The Ronald O. Perelman Department of Dermatology Kaplan Comprehensive Cancer Center, New York University Medical School, New York NY 10016, USA*

[3]*Microbiology Department Universidade Federal do Rio de Janeiro, RJ, Brazil*

[4]*The College of Life Sciences Peking University, Beijing, China*

[5]*Departments of Urology and Microbiology, Kaplan Comprehensive Cancer Center New York University Medical School, New York, NY 10016, USA*

[6]*Veterans Administration Medical Center in Manhattan New York, NY, 10010, USA*

[7]*Biozentrum, M. E. Müller Institute for Structural Biology University of Basel CH-4056, Basel, Switzerland*

[8]*Departments of Pharmacology and Urology, Kaplan Comprehensive Cancer Center New York University Medical School, New York, NY 10016, USA*

**Corresponding author*

The luminal surface of mouse urothelium in contact with the urine is almost entirely covered with plaques consisting of uroplakin-containing particles that form *p*6 hexagonal crystals with a center-to-center distance of 16 nm. A combination of quick-freeze/deep-etch images and our previous negative staining data indicate that the head domain of the uroplakin particle, which is exposed without an extensive glycocalyx shield, interacts closely with the head domains of the neighboring particles, while the membrane-embedded tail domains are farther apart; and that urothelial particles and plaques are not rigid structures as they can change their configuration in response to mechanical perturbations. Based on these data, we have constructed three-dimensional models depicting the structural organization of urothelial particles and plaques. Our models suggest that the head-to-head interaction may play a key role in determining the shape and size of the urothelial plaques. These models can explain many properties of urothelial plaques including their unique shape, detergent-insolubility, and morphological changes during vesicle maturation.

Keywords: bladder epithelium; asymmetric unit membrane; uroplakin; urothelial plaque; urothelial differentiation

Abbreviations used: AUM, asymmetric unit membrane; UP, uroplakin; 3-D, three-dimensional; EF, exoplasmic fracture; EM, electron microscopy; PF, protoplasmic fracture.

E-mail address of the corresponding author: sunt01@mcrcr.med.nyu.edu

0022-2836/99/020595–14 $30.00/0

Introduction

The apical surface of mammalian urinary bladder epithelium is covered by numerous rigid-looking, scallop-shaped membrane plaques (0.2-0.5 μm in diameter). The plaque is structurally unique in that its outer leaflet, as seen in vertical ultra-thin cross-sections, is about twice as thick as the inner one, hence the term ''asymmetric unit membrane'' or AUM (Hicks, 1965; Koss, 1969; Porter & Bonneville, 1963). The thickened outer leaflet of the AUM consists of hexagonal arrays of protein particles (16 nm center-to-center distance) that protrude from the lipid bilayer into the luminal space. Negative staining coupled with image processing showed that each AUM particle contains 12 stain-excluding subdomains (Brisson & Wade, 1983; Hicks & Ketterer, 1969; Taylor & Robertson, 1984; Vergara *et al.*, 1969). Unlike the granular appearance of the apical surface, the cytoplasmic surface of AUM appears relatively smooth. Since urothelial plaques and their protein subunits, i.e. the uroplakins, are synthesized in large quantities only by terminally differentiated urothelial cells, the AUM can be regarded as a major urothelial differentiation product (Sun *et al.*, 1996). This highly specialized membrane is believed to serve as an exceptionally effective permeability barrier (Chang *et al.*, 1994; Hicks, 1966; Hicks *et al.*, 1974); as a mechanical anchorage site mediating binding of the cytoskeleton to the apical membrane surface (Staehelin *et al.*, 1972); and as a mechanism for adjusting the apical surface area through the reversible insertion and retrieval of the apical plaques (Hicks, 1965; Lewis & de Moura, 1982, 1984; Minsky & Chlapowski, 1978; Porter & Bonneville, 1963; Porter *et al.*, 1967).

Recent analyses showed that urothelial plaques are biochemically unique. These membranes are unusually stable in that they remain insoluble in a number of harsh conditions including 2% NP-40, 2% sodium sarcosine, 25 mM NaOH, 9 M urea, and 6 M guanidium chloride (Wu *et al.*, 1990). They contain four major integral membrane proteins called uroplakins. Uroplakins Ia (27 kDa) and Ib (28 kDa) harbor four potential transmembrane domains (Yu *et al.*, 1994), while uroplakins II (15 kDa) and III (47 kDa) have only one (Lin *et al.*, 1994; Wu & Sun, 1993). Only uroplakin III has a significant cytoplasmic tail of about 50 amino acid residues (Wu & Sun, 1993; Yu *et al.*, 1994). This is consistent with the finding that the epitopes of UPIa, Ib and II are found to be associated mainly with the luminal leaflet of AUM, while the epitopes of UPIII are associated with both the cytoplasmic and luminal leaflets (Wu *et al.*, 1990). These results suggest that uroplakins are integral membrane proteins, that the extracellular domains of uroplakins bind to one another tightly by forming the 16-nm luminal particles, and that the cytoplasmic tail of UPIII may mediate AUM-cytoskeletal interactions.

A central, unresolved issue relates to the shape of the AUM particle. Staehelin and co-workers studied rabbit AUM using freeze-etch techniques, and they concluded that each AUM particle consists of six cylindrical domains surrounding a central hole with the top of the cylinders protruding into the luminal space (Staehelin *et al.*, 1972). This model does not explain, however, why all the intramembranous particles remain associated with the exoplasmic fracture (EF) face. The model was later challenged by Robertson and Vergara, who suggested that the granules of the EF face were artifacts of fracturing (Robertson & Vergara, 1980). The overall shape of the AUM particle, especially its transmembrane domain, is therefore controversial. In addition, it is unclear whether a urothelial plaque is a rigid and intact entity, or if it can break up into smaller plaques. It is also unclear what forces are involved in determining the concave shape and final size of an AUM plaque. Finally, it remains unclear what converts the uroplakin-delivering vesicles from a discoidal shape in the deep cytoplasm to a fusiform shape as they move toward the apical membrane.

Here, we examined the structure of mouse urothelium using the quick-freeze/deep-etch specimen preparation technique which preserves particularly well the surface topography of membranes and of their fractured surfaces. The emerging results, in combination with our earlier negative staining data (Walz *et al.*, 1995), enabled us to build a three-dimensional (3-D) model of the AUM particle consisting of a large head and a narrower tail. The head, about 16 nm in diameter, consists of 12 interconnected subdomains forming a ''twisted-ribbon'', or propeller-shaped, structure with a central hole, with the six inner subdomains occupying a lower position in contact with the luminal leaflet of the lipid bilayer (Walz *et al.*, 1995). The tail is narrower, about 11 nm in diameter, and consists of six cylinders surrounding a central depression that becomes narrower as it approaches the luminal leaflet. Construction of a 3-D model of the urothelial plaque showed that the extracellular head of each AUM particle intercalates closely with six neighboring heads, suggesting an extremely tight head-to-head interaction. In addition, we demonstrate that physical bending of a plaque as occurring in *in vitro* resealed vesicles can lead to the deformation of AUM particles located at the fault lines yielding multiple, smaller plaques separated by newly formed inter-plaque or ''hinge'' areas. These results indicate that AUM particles and plaques can undergo dynamic structural changes, and that head-to-head interactions among neighboring AUM particles may play a central role in plaque formation and regulation.

Results and Discussion

The exoplasmic surface of mouse urothelial plaques: arrays of protruding particles

Although relatively little is known about the ultrastructure of mouse urothelium (*versus* other mammalian species such as rat and rabbit), existing data indicate that the ultrastructure of mammalian urothelia is highly conserved (Firth & Hicks, 1973; Wu *et al*., 1994). Consistent with this, we found that the terminally differentiated mouse urothelial umbrella cells contain an impressive density of cytoplasmic vesicles that undergo a discoid-to-fusiform morphological transition in cortical cytoplasm (Figure 1a). These vesicles, as well as the apical urothelial plaques, are decorated by antibodies to uroplakins, the major AUM protein subunits (Figure 1b). When examined by the quick-freeze/deep-etch technique, which preserves the native, minimally perturbed membrane surface, both the apical plaques and the luminal surface of fusiform vesicles are characterized by arrays of particles (Figure 1c and d).

Image processing revealed a highly organized hexagonal array of particles with a center-to-center distance of 16 nm (Figure 1e; Robertson & Vergara, 1980; Staehelin *et al*., 1972). In sharp contrast, a similarly prepared frog bladder epithelial specimen can be seen to be covered with a thick forest of filamentous glycocalyx (Figure 1f) indicating that such a delicate glycocalyx structure, if it exists on mouse urothelial plaques, should be demonstrable by the quick-freeze deep-etch procedure. This result suggests that the apical surface of the 16-nm AUM particles, which contain mainly uroplakins including UPIa and Ib that we showed earlier can serve as the receptors for the type-1 fimbriated *E. coli* (Wu *et al*., 1996), is directly exposed to urine and to invading bacteria without being shielded by an extensive glycocalyx network. Our result does not rule out the possibility, however, that bacterial attachment to the urothelial receptors may be hindered by urinary mucopolysaccharides or glycoproteins, either as soluble urine components or after they have coated the surface of the urothelial plaques.

The exoplasmic fracture (EF) face: arrays of exposed tails of the AUM particles

When the lipid bilayer of AUM is split by freeze cleaving, the exposed exoplasmic fracture face (the EF face; Figure 2a) is characterized by particles that, like the luminal particles, form hexagonal arrays with a center-to-center distance of 16 nm (Figure 2b-e; Staehelin *et al*., 1972). As part of the exoplasmic or luminal leaflet structure, these particles, which are originally embedded in the lipid bilayer, are contiguous with the particles of the luminal surface. The intramembranous portion of the AUM particle is, however, only approximately 10-11 nm in diameter and is therefore significantly smaller than the apical AUM particles which have a diameter of 16 nm. In some particularly well resolved images the intramembranous portion of the AUM particle can be seen to consist of six subdomains surrounding a central depression (Figure 2f).

The protoplasmic fracture (PF) face exhibits complementary pits

The newly exposed inner surface of the protoplasmic leaflet (PF face) is characterized by a fine, hexagonal array of shallow pits (box in Figure 3a) with a center-to-center distance of 16 nm (Staehelin *et al*., 1972). Image processing revealed that each pit contains a central elevation (Figure 3, inset; see also Robertson & Vergara, 1980) which complements the central depression of the EF particles (Figure 2f). The overall physical dimensions and pattern of the PF face therefore complement quite well those of the exposed EF face, even though the PF pits appear to be somewhat shallower as has been noted by several earlier investigators (Robertson & Vergara, 1980; Staehelin *et al*., 1972).

The protoplasmic surface is smooth

Although occasionally one can see the outline of some underlying AUM particles bulging slightly through the protoplasmic surface (the P face) of AUM, by and large this surface of the AUM is smooth (Figure 2c; Brisson & Wade, 1983; Robertson & Vergara, 1980; Severs & Warren, 1978; Staehelin *et al*., 1972). Some intermediate filaments seem to attach tangentially to the P face (Figure 2c), but the interaction is not extensive and it is possible that this binding is mediated by delicate bridges as proposed by Staehelin *et al*. (1972).

The AUM particle consists of a large head and a narrower tail: a model

A major uncertainty in the area of the AUM field relates to the overall size and shape of the AUM particle. We have shown previously (Walz *et al*., 1995) by negative staining coupled with image analysis that each AUM particle consists of a head portion (the head) that is approximately 16 nm in diameter, and contains six inner and six outer subdomains interconnected forming a propeller- or ''twisted ribbon''-like structure (Figure 4a, b and c reveal its top, side and bottom view, respectively). While the six outer subdomains are elevated and are therefore spatially separated from the lipid bilayer, the six inner subdomains occupy a lower position forming six direct contact areas with the lipid bilayer (Walz *et al*., 1995). These six feet cover a diameter of about 10.8 nm, which fits quite well with the 10 to 11 nm diameter of the transmembranous domain (the tail) that is visible on the EF face of the AUM membrane (Figure 2). Since our data indicate that the tail consists of six cylinders par-

tially fused with one another surrounding a central depression, a model was constructed in which the six feet of the head are in register with the top of the six tail subdomains (Figure 4d, e and f show the top, side and bottom view of the model, respectively).

An important feature of our model, as depicted later in Figure 5d, is that the very bottom of the six

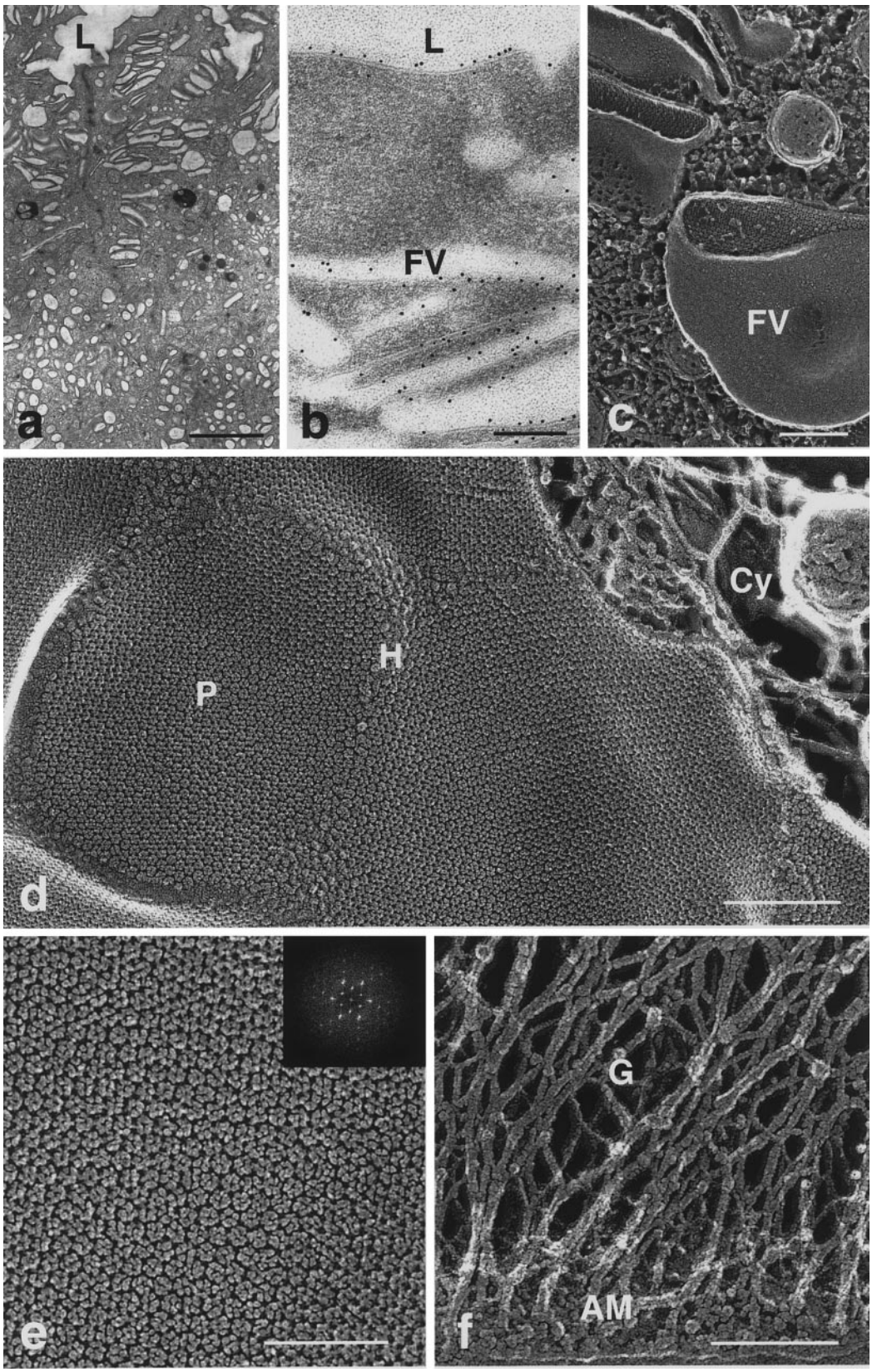

Figure 1 *(legend opposite)*

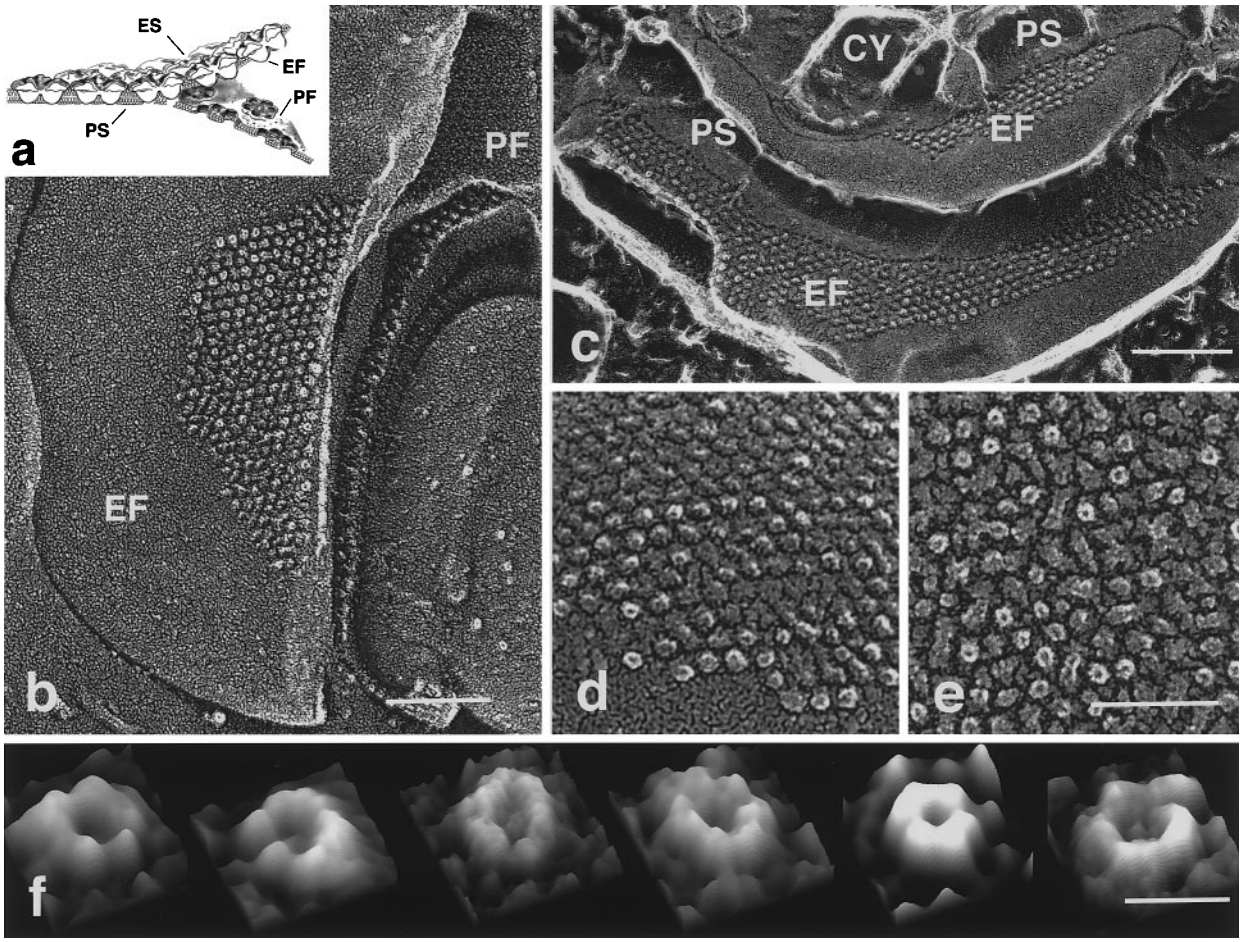

Figure 2. The surface views and freeze-fracture faces of mouse AUM plaques. a, A diagram defining the exoplasmic surface (ES), protoplasmic surface (PS), exoplasmic fractured surface (EF), and the protoplasmic fractured surface (PF) of the AUM. b, The EF of a cytoplasmic fusiform vesicle in a (rotary shadowed) replica of an unfixed, quick-frozen, and unetched specimen showing a well-aligned hexagonal array of particles, about 11 nm in diameter, with a center-to-center distance of about 16 nm. c, The exposed PS and EF faces of two adjacent fusiform vesicles of a fixed and QFDE specimen revealing well-organized, hexagonal arrays of 11-nm particles. The PS of the vesicles appears relatively smooth. Some cytoskeletal elements (Cy) appear to be attached to this area. d and e, EF faces of unfixed (d) and fixed (e) cytoplasmic vesicles showing the hexagonal arrays of 11-nm particles. During the splitting of the two halves of the membrane the intramembrane domain of the AUM particles showed some irregularities in shape and height suggesting that they were slightly deformed. Note the central depression at the tips of many particles. f, Surface plots of six 11-nm EF-face particles selected from b-e showing six subdomains surrounding a deep depression. The scale bars represent: b and c, 0.15 μm; d and e, 60 nm; and f 10 nm.

transmembrane subdomains of the tail protrudes into the cytoplasm. This was based on several considerations. First, as we have shown earlier, uroplakins are integral membrane proteins with cytoplasmic domains. While the putative cytoplasmic domains of UPIs and UPII are extremely small (<15 amino acid residues), that of UPIII contains 50 amino acid residues consistent with EM

Figure 1. The structural organization and luminal surface topography of mouse urothelium. a, A transmission electron micrograph showing the accumulation of discoidal and fusiform vesicles in lower and upper cytoplasm, respectively, and the covering of the luminal (L) cell surface by numerous plaques. b, Immunogold-labeling of the luminal surface and fusiform vesicles (FV) by a rabbit polyclonal antiserum to total bovine uroplakins (Wu *et al.*, 1990; Yu *et al.*, 1990); most of the gold particles are associated with the luminal side of the AUM plaques consistent with the known transmembrane topology of the uroplakin molecules. c-e, Quick-freeze deep-etch (QFDE) and rotary shadowed images of mouse bladder urothelium. c, The luminal surface of a fusiform vesicle is lined by 16-nm protein particles. d, An overview showing several crystalline plaques (P) interrupted by hinge areas (H). The upper right corner is an area where the apical surface membrane has been cross-fractured and the cytosol water etched thus exposing the underlying cytoskeleton (Cy). e, A high magnification image of the urothelial plaque and its fast Fourier transform (inset) showing the hexagonal symmetry of the packing and the twisted hexagonal symmetry of individual particles. f, A QFDE image of the apical membrane (AM) of frog bladder epithelium showing an extensive network of glycocalyx filaments (G) on its surface. The scale bars represent: a, 2 μm; b-d, 0.2 μm; e and f, 0.1 μm.

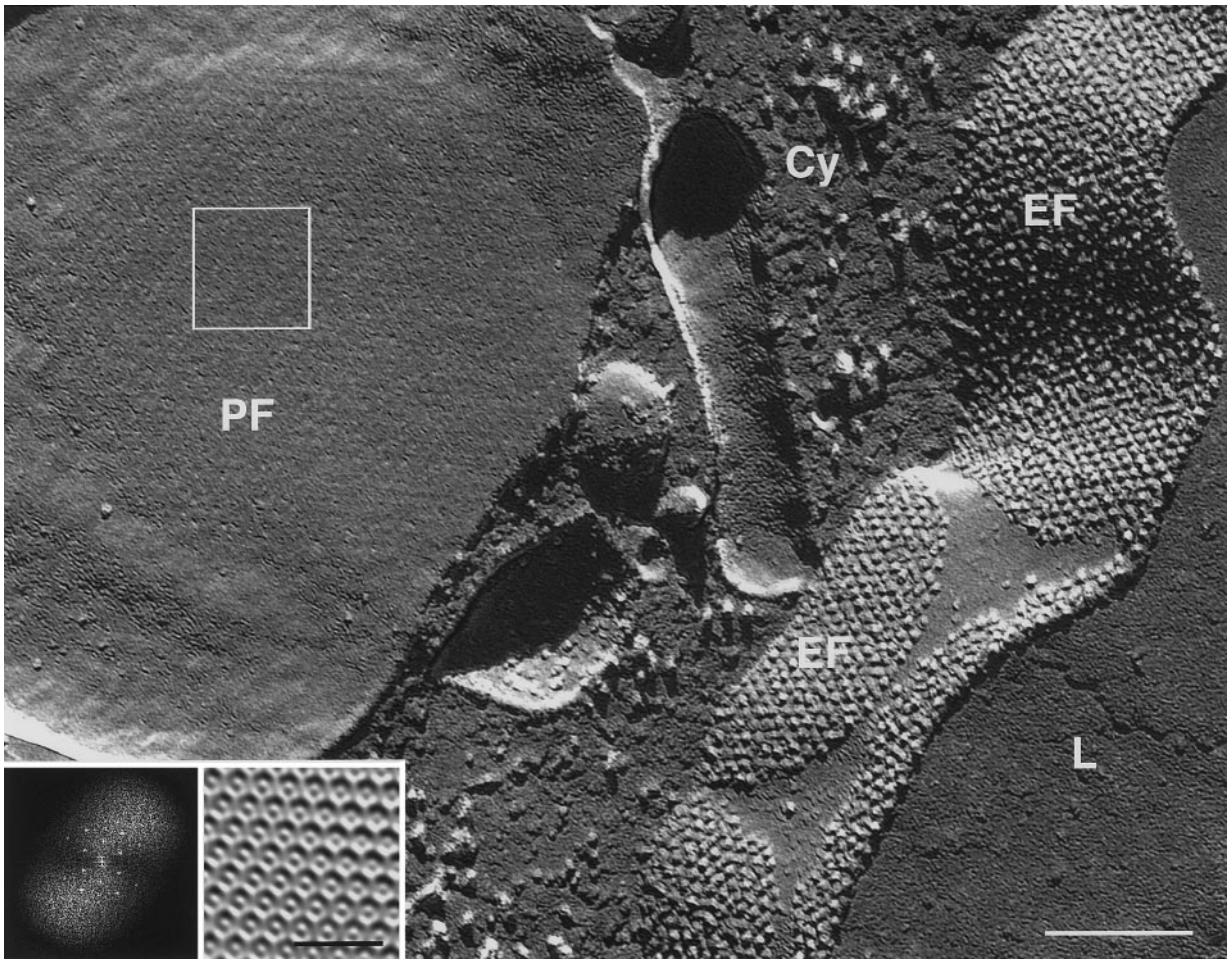

Figure 3. The structure of the protoplasmic fracture face (PF) of the mouse urothelial plaques. Electron micrograph of a unidirectionally shadowed replica of an unfixed, quick-frozen bladder. Note the EF faces of the several apical plaques (right) containing hexagonal arrays of 11 nm particles, and the PF face of a large fusiform vesicle (left) showing hexagonal arrays of shallow pits. A fast Fourier transform of the selected square of the PF face is shown in the inset to the left. The inset to the right shows an image of the inverse fast Fourier transform after a mask was applied to remove the noise which is due to the irregular shape of the grains of the platinum replica. Note the hexagonal arrays of pits with a center-to-center distance of 16 nm. Also note that in the center of each pit there is a small nipple-like elevation that fits well with the central depression at the tips of the 11 nm particle of the EF face. The scale bar represents 0.20 μm; and that in the inset 50 nm.

localization data revealing the exposure of some of the UPIII epitopes on the cytoplasmic side of AUM (Lin *et al*., 1994; Wu *et al*., 1990; Wu & Sun, 1993; Yu *et al*., 1994). Second, the P face of the AUM is known to be relatively smooth in keeping with the relatively small, cytoplasmically exposed domains of AUM particles (Figure 2c; Brisson & Wade, 1983; Robertson & Vergara, 1980; Severs & Warren, 1978; Staehelin *et al*., 1972). Third, the fact that, in this model, the lipid that fills up the central depression of the tail domain is connected at six points with the lipid moiety surrounding the particle can explain the PF pattern characterized by a contiguous sheet of lipid with a nipple-like elevation located at the center of each pit (Figure 3).

The physical dimensions of the model, as shown in Figures 4 and 5, are in general agreement with existing data. Overall, the head domain of the model, based on negative staining data (Walz *et al*., 1995), is better resolved than the tail. Based on a center-to-center distance of 16 nm, the maximal diameter (tip-to-tip) and the height of the particle are 16.8 nm and 5.5 nm, respectively (Figure 4d-f). The diameter of the tail domain, which covers the six feet of the head domain (Figure 4e and f), is 10.8 nm. We are less certain about the length of the transmembrane domain embedded in the lipid bilayer. We tentatively assigned a value of 4 nm based on the fact that lipid bilayers of a wide range of tissues with divergent lipid composition are of rather uniform thickness which almost never exceeds 4 nm (Johnson *et al*., 1991; Knoll *et al*., 1981; Seelig & Seelig, 1974), and that the tail domain does not appear to significantly protrude from the lipid bilayer on the cytoplasmic face. This value is considerably smaller than the 7.5-nm value based on transmission electron microscopy (Robertson & Vergara, 1980) which is, however,

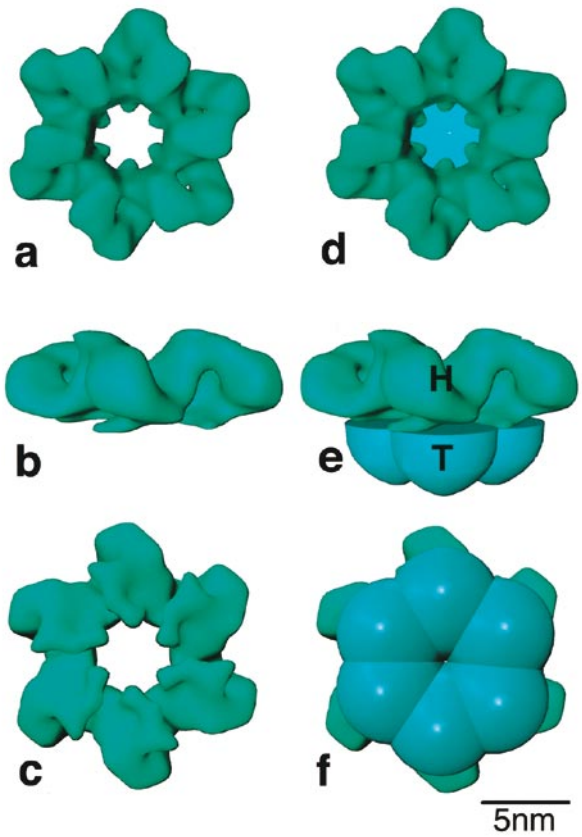

Figure 4. 3-D reconstruction of the 16-nm urothelial particle. a, Top, b, side and c, bottom view of a model of the 16-nm particle that protrudes from the lipid bilayer as we determined previously by negative staining (Walz *et al*., 1995). Note in a the presence of six inner and six outer subdomains that are interconnected forming a ''twisted ribbon'' structure. Note in b and c that the six outer subdomains occupy a relatively elevated position and are therefore not in contact with the lipid bilayer. In contrast, the six inner subdomains form six ''feet'' (best visualized in the bottom view of the model in c) that are in direct contact with the lipid bilayer; these six feet are by definition contiguous with the transmembrane domains of the protein particle. d, Top, e, side and f, bottom views of a model of a complete 16-nm AUM particle. A transmembrane (TM) structure (roughly 11 nm in diameter and 4 nm tall) was attached to the bottom of the twisted ribbon structure. Images such as those shown in Figure 2f suggest that this TM structure consists of six cylinders surrounding a central depression that becomes narrower towards the luminal side of the lipid bilayer (f). In this model we aligned the six TM cylinders with the six inner subdomains of the twisted-ribbon-shaped head portion (e and f); we cannot, however, rule out the possibility of skewing. While the model of the head domain is depicted at 25 Å resolution, the precise shape and diameter of the lipid-embedded tail domain are less certain due to the relatively low resolution of the freeze-etch data. The physical dimensions of the model, based on a center-to-center distance of 16 nm (Walz *et al*., 1995), are: maximal diameter (tip-to-tip) 16.75 nm; height of the luminally exposed head domain, 5.5 nm; diameter of the tail domain, 10.8 nm; and the height of the transmembrane domain that was embedded in the lipid bilayer, 4 nm (see the text). The scale bar represents 5 nm.

prone to artificial shrinkage or expansion. Future adjustment of the tail length will not, however, significantly affect any of the important features of our model (see below).

Relationships between our AUM model and two earlier models

(i) Model by Staehelin *et al*. (1972). While our freeze-fracture data are in excellent agreement with

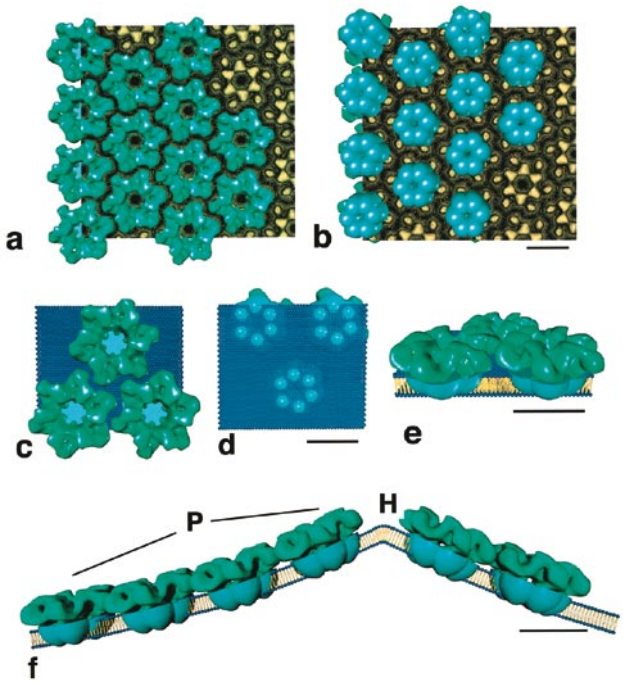

Figure 5. 3-D reconstruction of a urothelial plaque. a, The top view of a model in which several 3-D twisted-ribbon models of the head domain of the AUM particle were fit onto a two-dimensional AUM stain-exclusion map. b, The bottom view of the model showing the fitting of the models of the transmembranous (TM) portion of the AUM particle. The top c, bottom d, and slanted side e view of three particles that are embedded in a 4-nm thick lipid bilayer, showing the intercalated and close interactions among the head domains of the neighboring AUM particles. Note in d that the tail domains of the neighboring AUM particles are, in contrast, relatively far apart from one another and are therefore unlikely to interact with one another tightly. f, The side view of two model plaques (P) adjoined by a hinge area (H) illustrating the head-to-head interaction among neighboring AUM particles. We hypothesize that the head-to-head interaction between neighboring AUM particles results in a bend (that is 5° out of the plane in this diagram for illustration purpose) which results in the formation of a concave plaque. While the addition of a particle to the edge of an existing plaque may be energetically favored, this is counterbalanced by local surface tension which limits the extent by which the edge of an expanding plaque can protrude from the cell surface. The balance between these two opposing forces may thus limit the maximal number of particles that can participate in forming a single plaque. The scale bars represent 10 nm.

those of Staehelin *et al*. (1972), our model differs from theirs in several important aspects. In our model, we depicted the head domain of the AUM particle as being bulkier than the tail domain, while Staehelin *et al*. (1972) envisioned each particle as a ring of six simple cylinders of uniform diameter with the top protruding from the luminal surface. Therefore, their model cannot explain why the AUM particles are exclusively associated with the EF face in the freeze-fracture replicas. In addition, our model takes into account the negative staining data which resolved the head domain to a higher resolution (ca 25 Å) than Staehelin's model, that was based only on freeze-fracture data. By incorporating the twisted ribbon model of the head domain, our model uniquely demonstrates the close intercalating relationship among the heads of neighboring particles, while that by Staehelin *et al*. (1972) implies that the head-head and tail-tail interactions are of equal importance in AUM formation.

(ii) Model by Robertson & Vergara (1980). Our results and those of Staehelin *et al*. (1972) are inconsistent with those of Robertson & Vergara (1980, 1982) who thought that the particles on the EF face were artifacts, since their height was greater than the total thickness of the AUM, and since the EF face was not precisely complementary to the globular lattice of the PF face (Robertson & Vergara, 1980, 1982). Based on our data, we disagree with this interpretation. First, we confirmed that the transmembrane domain of the AUM particle on the EF face can indeed be artificially lengthened by freeze-fracturing and can be morphologically heterogeneous due to plastic deformation; this problem becomes particularly apparent in glutaraldehyde-fixed specimens (Figure 2e). However, the particles of the non-fixed specimens are more reproducible and show good complementarity to the PF face in their pattern, diameter, and lattice constant of the hexagonal lattice, as well as in their detailed shape (e.g. a central depression at the tip of the EF particle *versus* a central nipple-like elevation in the corresponding PF pit; Figures 2 and 3). Second, although the pits of the PF face are shallower than the tops of the EF face particles, this may be explained by several factors: (a) while the deposition of platinum particles during the rotary metal shadowing process tends to increase the height of an elevated structure, it decreases the depth of pits thus making them shallower; and (b) the rim of the pits, containing almost certainly pure lipid (Figure 3), may be particularly susceptible to shrinkage or etching damages (Robertson & Vergara, 1980; Severs & Warren, 1978; Staehelin *et al*., 1972). Third, the fact that the uroplakins are integral membrane proteins possessing transmembrane domains is inconsistent with Robertson and Vergara's model, whose central feature is that the AUM particles should fracture through the middle of the lipid bilayer yielding what they called a ''smooth'' EF pattern (which does not at all complement the PF face). Finally, as acknowledged by Robertson & Vergara (1980), the granular pattern is by far the predominant EF pattern seen in whole cells. Taken together, these considerations strongly suggest that the granular EF pattern (Figures 2b-d and 3a; Staehelin *et al*., 1972) reflects quite faithfully the overall shape of the transmembrane domain of the AUM particle *in vivo*.

Implications of our AUM model

Our model, as shown in Figure 4, has several implications:

(i) With a relatively large head domain protruding into the lumen of the AUM, plus the fact that these heads intercalate into one another (Figure 5a and c; and see below), our model explains why, when the AUM membrane is freeze-fractured, the entire array of AUM particles remains associated with the EF face (Figures 2b-d and 3a), leaving only complementary footprints of the tail domains on the PF face (Figure 3).

(ii) Since the head domain harbors a central hole all the way down to the luminal surface of the lipid bilayer, the fact that the tail domain also has a depression (even though it seems to be lipid-filled and its diameter becomes progressively smaller towards the luminal leaflet of the lipid bilayer) is interesting. Such a conical hole/depression can be seen in some of the AUM particles when viewed on edge in freeze-etched preparations (Figure 1d and data not shown). The presence of a protein-poor central depression in the transmembrane portion of the AUM particle raises intriguing questions as to whether the AUM particle is designed mechanically to twist like a camera shutter, resulting in a change in some physical parameters including the surface area it covers, or whether it contains a small and as yet uncharacterized channel.

(iii) Based on chemical crosslinking data, we have suggested earlier that uroplakin Ia (or Ib) occupies the six inner subdomains, while UPII (or UPIII) occupies the six outer subdomains of the AUM particle (Wu *et al*., 1995). The putative association of UPI subunits, that have four transmembrane domains (*versus* UPII and UPIII which have only one), with the inner six subdomains that are in contact with the lipid bilayer makes structural sense in terms of ease of inserting the transmembrane domains (TMDs) of these UPI molecules into the lipid bilayer (Lin *et al*., 1994; Wu *et al*., 1990; Wu & Sun, 1993; Yu *et al*., 1994).

Importance of head-head interaction in AUM formation

To better understand how the AUM particles interact with one another, we built a 3-D model of

a urothelial plaque. Using a Silicon Graphics computer program, we aligned the 12 subdomains of the head portion of the above model with those on a two-dimensional stain-exclusion pattern of an AUM (that had been adsorbed onto a grid with the luminal side up; Figure 5a; Walz *et al*., 1995). We then flipped the model upside down, and aligned the six subdomains of a tail domain with the six inner subdomains of the head (Figure 5b). Subsequent replacement of the 2-D stain-exclusion pattern by a lipid bilayer allowed us to see the 3-D spatial relationships among the neighboring AUM particles (Figure 5c-e). This model showed clearly that the head domain of each AUM particle intercalates with the heads of six neighboring particles thus forming a tightly packed complex (Figure 5c-e). In contrast, the narrower tail domains are relatively far apart and are separated from one another by many lipid molecules (Figure 5c-e).

This 3-D model of the urothelial plaque has several implications:

(i) A tight head-to-head interaction, which apparently involves protein-protein interactions among the extramembranous domains of the uroplakins, may explain the extraordinary insolubility of AUM plaques in a large number of detergents including 2% NP40 and 2% Sarkosyl (Liang *et al*., 1998; Wu *et al*., 1990).

(ii) Given the fact that AUM plaques represent 2-D crystals of uroplakins which are integral membrane proteins, the 55% lipid content of AUM was surprisingly high (Caruthers & Bonneville, 1977). A related, puzzling feature of AUM is that spin label studies showed that the highly organized AUM proteins do not seem to significantly perturb the hydrophobic core of the lipid bilayer (Vergara & Chesnut, 1983). The fact that most of the uroplakin protein domains form an extracellular head, that are excluded from the lipid bilayer and are anchored into the bilayer *via* a relatively thin tail, can easily explain these observations. In this regard, purified AUM has been shown to have a rather unusual lipid composition with cerebroside as a major component (Stubbs *et al*., 1979). Such a high concentration of unusual lipids in AUM suggests that lipids, thus far largely ignored, may play an important role in AUM structure and function.

(iii) The fact that head-to-head interaction may account for most of the direct interaction between neighboring particles implies that such an interaction plays a key role in determining the size and shape of the urothelial plaques. For example, if the binding between two neighboring particles occurs in such a way that it creates a small curvature of the plaque, as schematically shown in Figure 5f, in which this angle is arbitrarily set at 5° for the purpose of illustration, this will create a concave or scallop-shaped plaque. While adding another particle to the edge of an expanding plaque may be energetically favored from a protein-protein binding point of view, this interaction may be counterbalanced by surface tension which wants to minimize the protrusion of the cell surface. Such a balance between plaque expansion and local cell surface tension may be a critical factor in determining the final size and shape of an AUM plaque (Figure 5f).

(iv) In terminally differentiated urothelial (umbrella) cells, almost all the discoid AUM vesicles, which are accumulated in the deep cytoplasm, become fusiform as they move close to the apical membrane (Figure 1a). This can be explained by the fact that the density of AUM particles is relatively low in the immature vesicles (Severs & Hicks, 1979); in this situation the surface tension dominates, resulting in the formation of a spherical vesicle. When the number of AUM particles increases in the maturing vesicles (Severs & Hicks, 1979), they form large plaques through head-to-head interactions; under this circumstance the plaque formation becomes the dominant force, hence the conversion into fusiform vesicles.

(v) Although in our 3-D model of the urothelial plaque (Figure 5c) it may appear that each propeller-shaped head is separated from its six neighbors by a space that is uniform in width, detailed analysis of the 2-D stain-exclusion pattern showed that the tip of each outer domain is connected through a thin bridge with that of a neighboring head (Walz *et al*., 1995). Consistent with this, we have recently demonstrated that UPII, putatively associated with the outer six subdomains, can be crosslinked to UPII of a neighboring particle (Wu *et al*., 1995). It is therefore possible that head-to-head interaction specifically involves the tip of the six outer subdomains that are elevated from the lipid bilayer.

Morphological changes of the AUM particles in areas of new hinge formation

The apical surface of mouse urothelium is almost completely covered by AUM plaques that are 600-900 nm in diameter containing 1400-3000 particles, with only minimal discontinuities consisting of rows of deformed particles usually located along the hexagonal lattice lines (Figure 1d; see below). This observation is consistent with that by Hicks & Ketterer (1969, 1970) who reported that 100% of the rat ureter urothelial surface is covered by AUM plaques, but differs slightly from that by Staehelin *et al*. (1972) who found that only 75% of the rabbit urothelial apical surface is lined by the plaques.

Although it has been assumed previously that the AUM plaque is a rigid structure, it can apparently undergo major structural rearrangements (Figure 6). Figure 6a shows an experimentally produced vesicle formed by the *in vitro* re-sealing of a piece of apical surface membrane containing several AUM plaques. This resulted in the formation of a large, inverted vesicle (ca 0.8 μm × 1.6 μm) with its luminal surface facing outside. This and

many other isolated AUM vesicles contained small plaques containing an average of 100-400 particles (*versus* 1400-3000 particles of the native plaques) that are separated by faults that are formed along the hexagonal lattice (Figure 6b-e). Presumably these faults were formed in response to a greatly

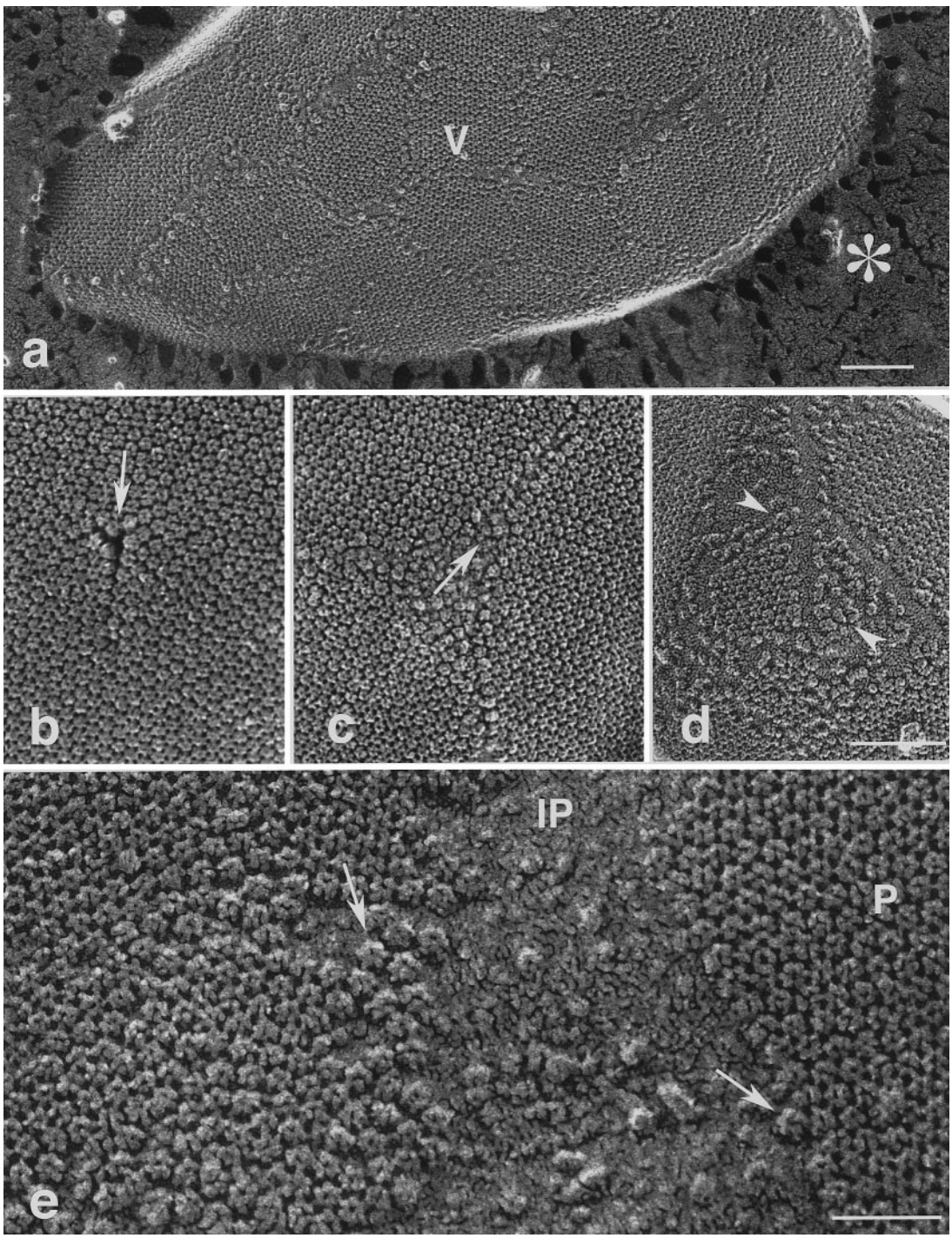

Figure 6. Deformation of AUM protein particles and the formation of new hinge areas in an *in vitro* re-sealed mouse urothelial surface membrane vesicle. a, A vesicle formed by the re-sealing of a large apical cell surface membrane probably consisting of several plaques. The 16-nm particles of this vesicle are exposed on the surface facing the surrounding ice (*); b-e, Higher magnification pictures showing, b, the junctional area of three converging, small faults (arrow marks the converging point) developed along the hexagonal lattice lines; c, the junctional area of three faults each along the hexagonal lattice lines showing the deformation of many 16-nm particles (arrow); d, an area with most of the particles already deformed (arrowheads) and physically separated from one another even though some small patches of particles still remain aggregated; e, an interplaque (IP) area that has become largely particle-free with surrounding particles undergoing desegregation (arrows). The scale bars represent a 0.15 μm; b-d, 0.1 μm; e, 50 nm.

increased surface tension in these vesicles in comparison with the intact cell surface. A highly reproducible feature of these newly formed faults is the presence of many deformed AUM particles that have lost their characteristic propeller shape and height (Figure 6d and e). Such deformed particles can also be seen *in vivo* as a predominant feature of the inter-plaque or hinge areas in unperturbed, native mouse urothelial surface (Figure 1d), suggesting that particle deformation may play a role in hinge formation both *in vivo* and *in vitro*.

These results suggest that the AUM particle is not a rigid structure, and that disruption of its association with neighboring particles in a hexagonal array is associated with major conformational changes of the particle resulting in the formation of new, relatively particle-free, hinge areas. The detailed structural basis of these changes is unclear.

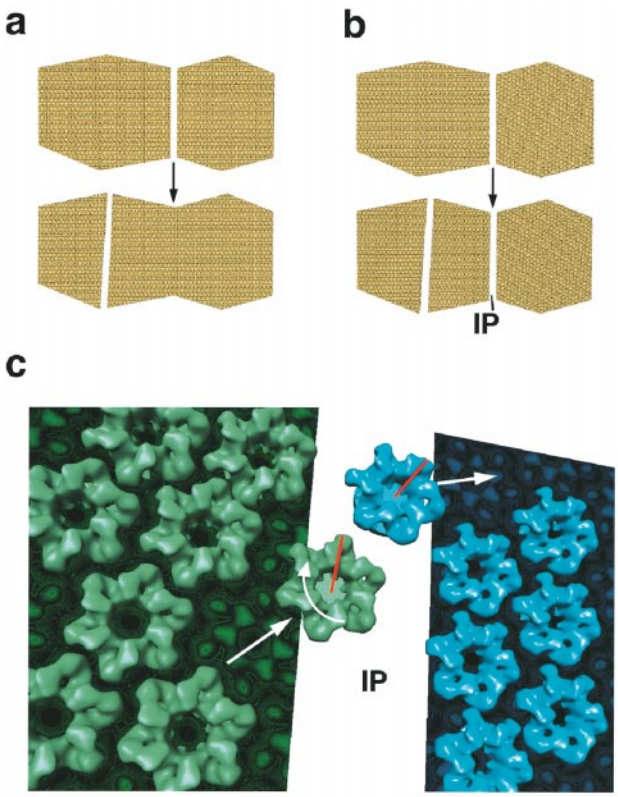

Figure 7. Two possible mechanisms by which AUM particles may redistribute among neighboring plaques. a and b, The breaking up of a large plaque and the fate of the resultant smaller plaques. As demonstrated in Figure 6, a plaque can break up into smaller plaques separated by a new, relatively particle-free hinge area. It is unknown whether the newly formed plaques will remain as small entities or whether they can fuse with some neighboring plaques forming larger ones. It is hypothesized here that two plaques can fuse to become a larger one (i) if the lattices of the two neighboring plaques are aligned and (ii) if the size of the resultant new plaque is within the limit determined by the balancing forces of head-to-head interaction *versus* local surface tension a. On the other hand, if the lattices of two neighboring plaques are not aligned, or if the combined size of the two plaques is too large, these two plaques will remain separated by an interplaque (IP) area, b. c, Even if two neighboring plaques remain separate (in this case due to the fact that their lattice lines deviate by 30° which is the maximum for two neighboring, 6-fold symmetrical plaques), individual AUM particles may be able to dissociate from one plaque, realign (in this case 30°) and then fuse with the neighboring plaque. These two models emphasize the dynamic behavior of urothelial plaque (a and b) and its individual particles, c.

Rearrangement of urothelial plaques: a ''plaque equilibrium'' hypothesis

When a plaque is divided into two smaller ones, as illustrated schematically in Figure 7a and b, what is the fate of the resultant smaller plaques? Will they remain separated or can they fuse with some neighboring plaques? Although we do not yet have an answer, we hypothesize that the outcome may depend on the size and lattice alignment of the plaques. If the lattice of a newly formed plaque is aligned with that of a neighboring plaque, and if the sum of the surface areas of the two plaques is within the limit dictated by the balance between head-to-head interaction *versus* local surface tension, it may be possible that these two plaques can fuse with one another forming a new, larger one (Figure 7a). Otherwise, this newly formed plaque may remain as a separate entity (Figure 7b). We further hypothesize that another way a plaque can achieve a dynamic equilibrium with its neighboring plaques is through the dissociation of some of its particles, which can then fuse (sometimes after an axial rotation) with neighboring plaques (Figure 7c); in this case the final sizes of all the plaques may still be governed by a balance between head-to-head interaction and surface tension.

This plaque-equilibrium hypothesis provides a possible solution allowing the fusion of subapical fusiform vesicles with the apical cell surface. Although relatively little is known about the mechanism by which a mature AUM vesicle fuses with the apical cell surface, it has been suggested that this involves the fusion between the hinge areas of the two partners (Staehelin *et al.*, 1972). If the bulk of the apical surface is covered by plaques (Figure 1) that are rigid and unavailable for fusion, this creates a major targeting problem as, by definition, the hinges of a great majority of the subapical fusiform vesicles are situated underneath nonfusible plaques. If our hypothesis is correct, i.e. if plaques are actually highly dynamic structures that undergo constant hinge formation and fusion (Figures 6 and 7), then any given area of the apical surface can become a hinge at some time depending on the maturation state and mechanical perturbation of the apical surface. This means that every fusiform vesicle may have equal access to an apical hinge area for fusion to occur. More data are needed to test this hypothesis.

Materials and Methods

Electron microscopy

For thin section transmission electron microscopy (EM), fresh bladders from adult Balb/c mice were cut into small pieces (<1 mm^2), fixed with 2.5% glutaraldehyde in 0.1 M sodium cacodylate buffer (pH 7.4), post-fixed with 2% (w/v) osmium tetroxide (OsO_4), and embedded in Epon 812 (Polysciences, Warrington, PA). For immunoelectron microscopy, tissues were fixed in 3% paraformaldehyde in 0.1 M sodium cacodylate buffer containing 4% (w/v) sucrose, dehydrated, and embedded in Lowicryl (Polysciences, Warrington, PA). Sections were incubated with a rabbit polyclonal antiserum against total uroplakins of bovine urothelial plaques (Wu *et al.*, 1990; Yu *et al.*, 1990).

Quick-freeze/deep-etch

Samples were fast frozen by contact with the surface of a sapphire block cooled to −186 °C with liquid N_2 using a Life Cell CF-100 freezing apparatus, freeze-fractured and/or freeze-etched, followed by platinum and carbon evaporation to form replicas using a Balzers 300 Freeze Fracture Unit. The platinum evaporation gun was positioned at 30-45° for unidirectional shadowing and at 12-15° for rotary shadowing. Replicas were viewed with a Zeiss 902 EM equipped with an electron energy loss spectrometer. Images were generated using only the inelastically scattered electrons. The electron micrograph negatives were digitized using a Leaf 45 scanner (Leaf Systems, Southborough, MA). Image processing was performed using either the NIH Image program or the Digital Micrograph 3.1 (Gatan, Inc.).

For examination of intact bladder samples, a fresh mouse bladder was cut into halves, rinsed with distilled water, and directly quick-frozen in liquid nitrogen. Alternatively, the bladder halves were fixed with 2% glutaraldehyde, or fixed after they had been extracted briefly with 0.1% Triton X-100 in buffer A (30 mM Hepes (pH 7.1-7.4), 70 mM KCl, 5 mM $MgCl_2$, 3 mM EGTA, 0.1 mM 4-(2-aminoethyl)-benzensulfonyl fluoride (AEBSF), and 1 mM DTT) for five minutes at room temperature (Heuser, 1983). The samples were then processed for quick-freeze/deep-etch preparation (see below).

For examination of crude urothelial membranes, fresh mouse bladder was inverted, rinsed with ice-cold phosphate-buffered saline (PBS, pH 7.4), and the surface urothelium was scraped from the luminal surface with a blunt scalpel. The scraped urothelial sheets were suspended in PBS, collected by ten minutes centrifugation at 1500 *g* and 4 °C, and homogenized in buffer A. After 15 minutes centrifugation at 2500 *g* and 4 °C, the cell pellet was resuspended in buffer A, loaded onto a 1.6 M sucrose cushion (same buffer), and centrifuged for 20 minutes in a SW41 (Beckman) rotor at 16,000 rpm and 4 °C. The crude plasma membranes concentrated at the cushion interface were collected, and washed with buffer A by suspension and centrifugation. These total plasma membranes were then fixed for two hours with 2% glutaraldehyde in buffer A without AEBSF or DTT. After three rinses with distilled water, the samples were quick-frozen, deep-etched, and rotary or unidirectionally metal shadowed (Kachar & Reese, 1988).

3-D reconstruction, surface rendering, and molecular modeling

The 3-D stack of sections of the AUM particle was visualized and rendered by real-time isocontouring (Henn *et al.*, 1996). The program iso used in this work was developed in the Basel laboratory on a Silicon Graphics Impact computer. Showcase and Revo were used to build the initial graphs of the lipid bilayer and the 16-nm particle. Scene Viewer was used to construct the composites shown in Figures 4, 5 and 7. All three programs are part of the Irix 6.2 system software. In order to align the AUM particles in 3-D, texture mapping (Teschner *et al.*, 1994) was used. An image-processed 2-D map of negatively stained AUM plaques was used to generate a contiguous texture. This texture was glued on a plate which then served as an orientation guide to align the 3-D models of AUM particles (Figure 5).

Acknowledgments

This work was supported by National Institutes of Health grants (DK39753, DK47529 and DK49469 to T.-T.S.), by a Veterans Administration Merit Review Award (to X.-R.W.), by a grant from the Swiss National Science Foundation (3100-053028.97 to U.A.), by a predoctoral fellowship from the Schweizerische Chemie Stiftung (to D.S.), by the M.E. Müller Foundation of Switzerland, and by the Canton Basel-Stadt. We thank Gavin P. Riordan for technical assistance. We also thank Dr John E. Heuser of Washington University Medical School, St. Louis, for his contributions during the early phase of this work and Drs Brian Andrews of NINDS, NIH and Xiangpeng Kong of Skirball Institute of Biomedicine, New York University Medical School, for stimulating discussions.

References

Brisson, A. & Wade, R. H. (1983). 3-D structure of luminal plasma membrane protein from urinary bladder. *J. Mol. Biol.* **166**, 21-36.

Caruthers, J. S. & Bonneville, M. A. (1977). Isolation and characterization of the urothelial lumenal plasma membrane. *J. Cell Biol.* **73**, 382-99.

Chang, A., Hammond, T. G., Sun, T.-T. & Zeidel, M. L. (1994). Permeability properties of the mammalian bladder apical membrane. *Am. J. Physiol.* **267**, C1483-1492.

Firth, J. A. & Hicks, R. M. (1973). Interspecies variation in the fine structure and enzyme cytochemistry of mammalian transitional epithelium. *J. Anat.* **116**, 31-43.

Henn, C., Teschner, M., Engel, A. & Aebi, U. (1996). Real-time isocontouring and texture mapping meet new challenges in interactive molecular graphics applications. *J. Struct. Biol.* **116**, 92-96.

Heuser, J. E. (1983). Structure of the myosin crossbridge lattice in insect flight muscle. *J. Mol. Biol.* **169**, 123-154.

Hicks, R. M. (1965). The fine structure of the transitional epithelium of rat ureter. *J. Cell Biol.* **26**, 25-48.

Hicks, R. M. (1966). The permeability of rat transitional epithelium. Keratinization and the barrier to water. *J. Cell Biol.* **28**, 21-31.

Hicks, R. M. & Ketterer, B. (1969). Hexagonal lattice of subunits in the thick luminal membrane of the rat urinary bladder. *Nature*, **224**, 1304-1305.

Hicks, R. M. & Ketterer, B. (1970). Isolation of the plasma membrane of the lumenal surface of rat bladder epithelium, and the occurrence of a hexagonal lattice of subunits both in negatively stained whole mounts and in sectioned membranes. *J. Cell Biol.* **45**, 542-553.

Hicks, R. M., Ketterer, B. & Warren, R. C. (1974). The ultrastructure and chemistry of the luminal plasma membrane of the mammalian urinary bladder: a structure with low permeability to water and ions. *Phil. Trans. Roy. Soc. London*, **268**, 23-38.

Johnson, S. J., Bayerl, T. M., McDermott, D. C., Adam, G. W., Rennie, A. R., Thopmas, K. K. & Sackmann, E. (1991). Structure of an adsorbed dimyristoylphosphatidylcholine bilayer measured with specular reflection of neutrons. *Biophys. J.* **59**, 289-294.

Kachar, B. & Reese, T. S. (1988). The mechanism of cytoplasmic streaming in characean algal cells: sliding of endoplasmic filaments along actin filaments. *J. Cell Biol.* **106**, 1545-1552.

Knoll, W., Haas, J., Stuhrmann, H. B., Fuldner, H.-H., Vogel, H. & Sackmann, E. (1981). Small-angle neutron scattering of aqueous dispersions of lipids and lipid mixtures. A contrast variation study. *J. Appl. Crystallog.* **14**, 191-202.

Koss, L. G. (1969). The asymmetric unit membranes of the epithelium of the urinary bladder of the rat. An electron microscopic study of a mechanism of epithelial maturation and function. *Lab. Invest.* **21**, 154-168.

Lewis, S. A. & de Moura, J. L. (1982). Incorporation of cytoplasmic vesicles into apical membrane of mammalian urinary bladder epithelium. *Nature*, **297**, 685-688.

Lewis, S. A. & de Moura, J. L. (1984). Apical membrane area of rabbit urinary bladder increases by fusion of intracellular vesicles: an electrophysiological study. *J. Membr. Biol.* **82**, 123-136.

Liang, F. X., Kachar, B., Ding, M. X., Zhai, Z. H., Wu, X. R. & Sun, T.-T. (1998). Urothelial hinge as a highly specialized membrane: detergent insolubility, urohingin association, and in vitro formation. *J. Cell Sci.* submitted.

Lin, J. H., Wu, X. R., Kreibich, G. & Sun, T.-T. (1994). Precursor sequence, processing, and urothelium-specific expression of a major 15-kDa protein subunit of asymmetric unit membrane. *J. Biol. Chem.* **269**, 1775-1784.

Minsky, B. D. & Chlapowski, F. J. (1978). Morphometric analysis of the translocation of lumenal membrane between cytoplasm and cell surface of transitional epithelial cells during the expansion-contraction cycles of mammalian urinary bladder. *J. Cell Biol.* **77**, 685-697.

Porter, K. R. & Bonneville, M. A. (1963). *An Introduction to the Fine Structure of Cells and Tissues*, Lea and Febiger, New York.

Porter, K. R., Kenyon, K. & Badenhausen, S. (1967). Specifications of the unit membrane. *Protoplasma*, **63**, 263-274.

Robertson, J. D. & Vergara, J. (1980). Analysis of the structure of intramembrane particles of the mammalian urinary bladder. *J. Cell Biol.* **86**, 514-28.

Robertson, J. D. & Vergara, J. (1982). One kind of intramembrane particle is water soluble. *Biophys. J.* **37**, 199-201.

Seelig, A. & Seelig, J. (1974). The dynamic structure of fatty acyl chains in a phospholipid bilayer measured by deuterium magnetic resonance. *Biochemistry*, **13**, 4839-4845.

Severs, N. J. & Hicks, R. M. (1979). Analysis of membrane structure in the transitional epithelium of rat urinary bladder. 2. The discoidal vesicles and Golgi apparatus: their role in luminal membrane biogenesis. *J. Ultrastruct. Res.* **69**, 279-296.

Severs, N. J. & Warren, R. C. (1978). Analysis of membrane structure in the transitional epithelium of rat urinary bladder. 1. The luminal membrane. *J. Ultrastruct. Res.* **64**, 124-140.

Staehelin, L. A., Chlapowski, F. J. & Bonneville, M. A. (1972). Lumenal plasma membrane of the urinary bladder. I. 3-D reconstruction from freeze-etch images. *J. Cell Biol.* **53**, 73-91.

Stubbs, C. D., Ketterer, B. & Hicks, R. M. (1979). The isolation and analysis of the luminal plasma membrane of calf urinary bladder epithelium. *Biochim. Biophys. Acta*, **558**, 58-72.

Sun, T.-T., Zhao, H., Provet, J., Aebi, U. & Wu, X. R. (1996). Formation of asymmetric unit membrane during urothelial differentiation. *Mol. Biol. Rep.* **23**, 3-11.

Taylor, K. A. & Robertson, J. D. (1984). Analysis of the 3-D structure of the urinary bladder epithelial cell membranes. *J. Ultrastruct. Res.* **87**, 23-30.

Teschner, M., Henn, C., Vollhardt, H., Reilling, S. & Brickmann, J. (1994). Texture mapping: a new tool for molecular graphics. *J. Mol. Graphics*, **12**, 98-105.

Vergara, J., Longley, W. & Robertson, J. D. (1969). A hexagonal arrangement of subunits in membrane of mouse urinary bladder. *J. Mol. Biol.* **46**, 593-596.

Vergara, J. A. & Chesnut, D. B. (1983). A spin label study of the urinary bladder luminal membrane. *Biochim. Biophys. Acta*, **734**, 18-24.

Walz, T., Haner, M., Wu, X. R., Henn, C., Engel, A., Sun, T.-T. & Aebi, U. (1995). Towards the molecular architecture of the asymmetric unit membrane of the mammalian urinary bladder epithelium: a closed ''twisted ribbon'' structure. *J. Mol. Biol.* **248**, 887-900.

Wu, X. R. & Sun, T.-T. (1993). Molecular cloning of a 47 kDa tissue-specific and differentiation-dependent urothelial cell surface glycoprotein. *J. Cell Sci.* **106**, 31-43.

Wu, X. R., Manabe, M., Yu, J. & Sun, T.-T. (1990). Large scale purification and immunolocalization of bovine uroplakins I, II, and III. Molecular markers of urothelial differentiation. *J. Biol. Chem.* **265**, 19170-19179.

Wu, X. R., Lin, J. H., Walz, T., Haner, M., Yu, J., Aebi, U. & Sun, T.-T. (1994). Mammalian uroplakins. A group of highly conserved urothelial differentiation-related membrane proteins. *J. Biol. Chem.* **269**, 13716-13724.

Wu, X. R., Medina, J. J. & Sun, T.-T. (1995). Selective interactions of UPIa and UPIb, two members of the transmembrane 4 superfamily, with distinct single transmembrane-domained proteins in differentiated urothelial cells. *J. Biol. Chem.* **270**, 29752-29759.

Wu, X. R., Sun, T.-T. & Medina, J. J. (1996). In vitro binding of type 1-fimbriated Escherichia coli to uroplakins Ia and Ib: relation to urinary tract infections. *Proc. Natl Acad. Sci. USA*, **93**, 9630-9635.

Yu, J., Manabe, M., Wu, X. R., Xu, C., Surya, B. & Sun, T.-T. (1990). Uroplakin I: a 27-kD protein associated with the asymmetric unit membrane of mammalian urothelium. *J. Cell Biol.* **111**, 1207-1216.

Yu, J., Lin, J. H., Wu, X. R. & Sun, T.-T. (1994). Uroplakins Ia and Ib, two major differentiation products of bladder epithelium, belong to a family of four transmembrane domain (4TM) proteins. *J. Cell Biol.* **125**, 171-182.

Edited by W. Baumeisser

(Received 16 July 1998; received in revised form 29 September 1998; accepted 4 October 1998)